Chapter 1

Inelastic X-Ray Scattering as a Probe of the Transition Between the Hydrodynamic and the Single Particle Regimes in Simple Fluids

Alessandro Cunsolo

Additional information is available at the end of the chapter

http://dx.doi.org/10.5772/66126

Abstract

In the last few decades, the study of the spectrum of density fluctuations in fluids at the transition from the continuous to the single particle regimes has attracted an increasing interest. Although the shape of the spectrum is well known in these two extreme limits, no theory firmly predicts its evolution in the broad crossover region. However, the development of inelastic X-ray scattering (IXS) has substantially expanded the potentialities of modern spectroscopy, thus, providing an unprecedented detailed mapping of such a crossover. A better understanding of the line-shape evolution in this intermediate regime is deemed to improve our knowledge of all dynamical processes occurring in a fluid from macroscopic to microscopic scales. The aim of this chapter is to review some relevant experimental contributions brought about by IXS in this field since its development toward the end of past millennium.

Keywords: inelastic X-ray scattering, simple fluids, hydrodynamics, single particle limit, collective excitations

1. Introduction

In the last 50 years, the short-time collective dynamics of molecules in fluid and glassy systems has been in the focus of a thorough experimental, theoretical, and computational scrutiny, yet it still has many unsettled aspects. This mostly owes to the lack of a large-scale symmetry in the structure of these systems and to the often exceptionally complex movements of their microscopic constituents. Among various variables providing insight into the dynamic behavior of a disordered system, density fluctuations are a particularly well-suited subject to

study, as they can be directly accessed by several independent investigation methods. Indeed, the most significant advances made in the field of dynamics of liquids have been achieved thanks to the critical comparison of parallel experimental and computational results. In fact, both spectroscopy experiments and molecular dynamics simulations provide direct access to the Fourier transform of correlation functions between density fluctuations, i. e., the dynamic structure factor, $S(Q,\omega)$. This variable is a unique function of the energy, $\hbar\omega$, and the momentum $\hbar\vec{Q}$ exchanged between the probe and the sample in a scattering event; here $\hbar = h/2\pi$ with h being the Planck constant.

In general, the shape of $S(Q,\omega)$ is reasonably understood both at quasi-macroscopic distances, over which the fluid appears as a continuum, and at truly microscopic scales where instead the single particle dynamics is probed.

The evolution of the $S(Q,\omega)$ shape in the whole crossover between these two limits still represents a theoretical challenge. This particularly applies to the so-called "mesoscopic" regime, corresponding to distances and timescales roughly matching first neighboring molecules' separations and cage oscillations periods, respectively. From the experimental side, the study of $S(Q,\omega)$ in liquids at mesoscopic scales has been for long time an exclusive domain of inelastic neutron scattering (INS), a technique already in its mature phase, having been developed in the mid-1950s [1]. The complementary mesoscopic technique, inelastic X-ray scattering (IXS), is instead relatively young, since its first demonstration dates back to the last decade of the past millennium [2, 3]. Its implementation was enabled by the advent of synchrotron sources with unprecedented brilliance and by parallel advances in crystal optics fabrication. Furthermore, the improved performance of X-ray sources has greatly increased the level of statistical accuracy typically achieved by inelastic scattering measurements, thus enabling more detailed and physically informative modeling of the spetral shape. Across the years, this new spectroscopic tool allowed the scientific community to gain a deep-seated knowledge of the mesoscopic dynamics of disordered systems. Nowadays, IXS experiments have reached the level of statistical accuracy required for extremely detailed and informative line-shape analyses, thus representing a valuable test for the most advanced theories of liquid dynamics.

As a simple example of possible IXS applications, this chapter will provide a concise overview of relevant IXS investigations of the $S(Q,\omega)$ across the transition from the hydrodynamic to the single particle regimes. Looking at the available literature results from a global perspective has a relevant scientific interest since a better understanding of this crossover can shed further insight into the various dynamic events occurring in a fluid from macroscopic to microscopic scales.

2. Generalities on an inelastic scattering experiment

In a scattering experiment, a beam impinges on the sample exchanging with it, an energy of $\hbar\omega$ and a momentum of $\hbar\vec{Q}$. It can be shown that intensity measured in a spectroscopy

http://dx.doi.org/10.5772/66126

experiment from GHz frequencies [4] to THz ones [5–7] is proportional to the spectrum of density fluctuations, or dynamic structure factor:

$$S(Q,\omega) = \int_V d\vec{r} \int_{-\infty}^{+\infty} \left\langle \delta\rho(\vec{r},t)\delta\rho^*(\vec{r},0) \right\rangle \exp\left[i(\vec{Q}\cdot\vec{r} - \omega t) \right] dt \tag{1}$$

with $\delta\rho(\vec{r},t)$ being the space ($\vec{r}$) and time *(t)* dependent density fluctuation of the target sample within the volume *V*. The term $\delta\rho(\vec{r},t)$ appearing in Eq. (1) may represent either a spontaneous or a scattering-induced density fluctuation, in either case its amplitude is assumed small enough to induce a linear response on the target sample. Under this condition, the response of the latter can be expressed in terms of correlation functions calculated at its equilibrium. Note that for isotropic systems as liquids and glasses, only the amplitude $Q = |\vec{Q}|$ of the exchanged wave-vector $\vec{Q}$ counts, the actual direction being irrelevant. For this reason, while dealing with these systems, it is customary to express the dynamic structure factor as $S(Q,\omega)$ rather than $S(\vec{Q}, \omega)$.

Typically, in a scattering experiment the sample is kept at a constant temperature *T* and therefore the correlation function, defined by the symbol ⟨.....⟩, can be calculated as a thermal average over the initial states of the target atoms. For a classical system, this sum can be performed using the counting factor $n(E_I)=\exp(-\beta E_I)\Big/\sum_I \exp(-\beta E_I)$, with $\beta = 1/k_B T$, where E_I is the energy of the *I*-th initial state and k_B, the Boltzmann constant. From the above formula, one readily recognizes that the scattering of a plane wave at an energy (frequency) and a direction (wavevector) different from the initial ones is caused by a density fluctuation $\delta\rho(\vec{r},t)$. If, for instance, if the probe is visible light, the occurrence of a density fluctuation causes a local variation of the index of refraction, thereby disrupting the optical homogeinity of the medium. By virtue of the scattering event, according to the Huygens principle (see, e.g., [8]), the target sample becomes the source of spherical wave: $\psi_{sc} \propto e^{ikr}/r$ with *r* being the distance from the origin, that is the location of the probe-sample collision.

The photoms deviated at an angle 2θ, after passing through an analyzer filter are ultimately counted by the detector. If the latter intercepts only a very small portion of the solid angle, it can be safely assumed that the wavevector of photons impinging on its sensitive area is constant and orthogonal to the front wave (plane wave approximation). Consequently, the scattering process can be treated as a transition between two distinct plane waves.

Given the above general considerations, we can now attempt a course derivation of the frequency distribution of the scattering from a density wave to achieve a rough estimate of the shape of $S(Q,\omega)$.

As apparent from Eq. (1), $S(Q,\omega)$ is connected to density fluctuations through the space and time Fourier transform of their correlation function. Its determination thus provides a snapshot of this correlation function over timescale ~ ω^{-1} and distances ~ Q^{-1}. For small *Q* and ω, the target system is "perceived" by the probe as a continuous and homogeneus medium, whose dynamic response is averaged over long times. This continuous limit can be probed, for

instance, by illuminating the sample with the visible light beam emitted by a laser. In fact, Q values typical of visible light scattering measurements span the 10^{-3}–10^{-2} nm^{-1} range, corresponding to sub-μm to μm lengthscales. These distances are sufficiently smaller than the sample size, yet still much larger than first neighboring atoms' separations. Clearly, at these scales the detail of the microscopic structure and dynamics cannot be directly observed, since only long distances and times effects on the dynamics can be captured by the probe.

Over long distances density fluctuations in a liquid can, for instance, have the form of density (acoustic) waves propagating throughout the medium with the speed of sound, c_s. Since c_s is much smaller the speed of light in the medium a given density wave is "seen" by the incident photons as essentially static, i. e., stationary, perturbation.

We can now focus on the intensity scattered, e.g., by successive crests of the density wave, as illustrated in **Figure 1**. The interference between these successive reflections is constructive whenever the difference in their optical paths (namely, the two red segments in the scheme of **Figure 1**) equals an integer multiple of the incident wavelength in the medium. Considering the smallest of these integer numbers, one has:

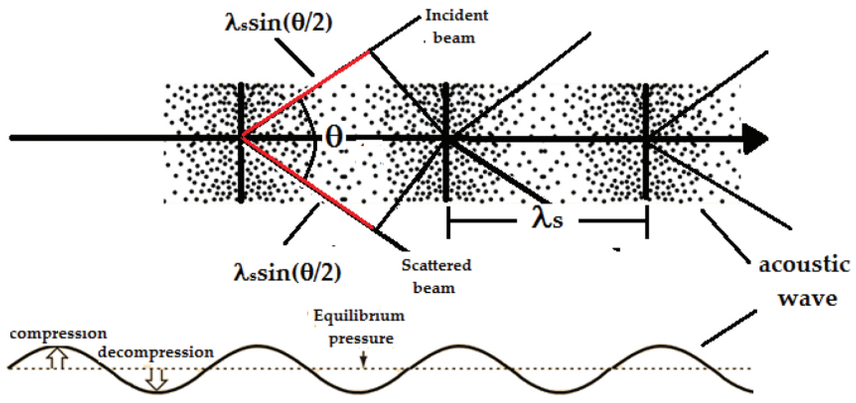

Figure 1. Schematics of the interaction between a density wave and a photon beam (see text) causing a scattering at an angle 2θ.

$$\frac{\lambda}{n} = 2\lambda_s \sin\vartheta = 4\pi \frac{c_s}{\omega_s} \sin\vartheta \tag{2}$$

where λ and λ/n are, respectively, the wavelength of light in vacuum and in the target medium, with n being the refractive index of the sample; furthermore, λ_s, c_s, and ω_s are the wavelength, the speed and the angular frequency of the acoustic wave with $\lambda_s = 2\pi c_s/\omega_s$. The scattering-genearted acoustic wave has a wavevector of amplitude amplitude = Q, therefore it propagates at a frequency $\omega_s = c_s Q$. From Eq. (2) it follows that the amplitude of the exchanged wavevector is $Q = (4\pi n/\lambda) \sin\theta$.

From a physical point of view, the acoustic wave can be considered as a source of scattered radiation traveling with a velocity c_s. As well known from Physics textbooks, the frequency of

http://dx.doi.org/10.5772/66126

the radiation emitted by a moving source is frequency-shifted by the Doppler effect. This ultimately causes $a \pm c_s Q$ offset of the frequency of scattered wave with respect to the one of the incident beam; here the signs "+" and "−" refer to the acoustic wave propagating toward or away from the detector, respectively. From these very general arguments, one can expect the frequency distribution of the scattered intensity, i.e., the spectrum, to be dominated by two peaks symmetrically shifted by an amount $\pm c_s Q$ from the center of the spectrum, $\omega = 0$.

These peaks are customarily quoted as "inelastic" insofar their energy is either lower or higher (by an amount $E = \hbar c_s Q$) than the energy of the impinging beam.

The two symmetric side peaks are named Brillouin peaks after their prediction by L. Brillouin in the early 1920s [9] and, as discussed in the following, their position and width convey insight, on the frequency and the lifetime of acoustic waves, respectively.

Let us now consider the case of diffusive, rather than propagating, density fluctuations. These can be for instance those generated by local temperature gradients causing transient density inhomogeneities. Their time evolution can be described by the Fick's law [10], which predicts a simple exponential time decay. The corresponding spectral shape is the Fourier transform of such an exponential law, namely a Lorentzian centered at $w = 0$. Since this position corresponds to the absence of energy-transfer, the corresponding peak is thus customarily referred to as quasi-elastic. Here the prefix "quasi-" alludes to the nonvanishing width of the peak and to its wings extending to the inelatic region of the spectrum ($w \neq 0$).

Since in general density fluctuations in a fluid can have either a diffusive, or a propagating character, one can anticipate that the spectrum of density fluctuations has a triplet shape composed by a quasi-elastic peak—connected to internal diffusive motions—and two symmmetric side peaks— arising from acoustic modes.

A physically more informative description of the spectral shape in the continuous limit requires a detailed knowledge of the thermodynamic and transport properties of the sample. As well assessed both experimentally and computationally, the hydrodynamic theory for continuous media can be consistently used to describe the spectral shape in this limit.

This theory stems from an explicit expression of the conservation laws of the density of mass, momentum, and energy of the target sample [4, 11]. These can be described by few independent equations, which, however, do not form a complete set unless complemented by two so-called constitutive equations: the Navier-Stokes equation and the heat transfer one. The spectrum of density fluctuation can be ultimately obtained through Fourier and Laplace transforms of this set of equations. The result can be conveniently expressed in terms of a hydrodynamic matrix, whose eigenvalues define the modes dominating the spectral shape. As shown in Ref. [4] these long-lived, or quasi-conserved, collective modes are customarily referred to as "hydrodynamic modes," and appear in the spectrum as a triplet, well approximated by the following expression:

$$S(Q,\omega) \propto A_h \frac{z_h}{\omega^2 + z_h^2} + A_S \left[\frac{z_S}{(\omega - \omega_S)^2 + z_S^2} + \frac{z_S}{(\omega + \omega_S)^2 + z_S^2} \right] + \\ + A_S b \left[\frac{(\omega - \omega_S)}{(\omega - \omega_S)^2 + z_S^2} - \frac{(\omega + \omega_S)}{(\omega + \omega_S)^2 + z_S^2} \right] \tag{3}$$

where the shape parameters ω_s, z_h and z_s represent the acoustic frequency and the inverse lifetime of the quasi-elastic and inelastic modes, respectively. All shape parameters in Eq. (3) are in general Q dependent, even if such dependence is not explicitly mentioned in the notation.

At low Q values, such a Q-dependence can be made explicit using a polynomial Q-expansion (see, e.g., [12]), which to the lowest order yields:

$$\omega_s \approx \omega_s^{hyd} = c_s Q \tag{4a}$$

$$z_s \approx z_s^{hyd} = \left[(\gamma - 1) D_T + \nu_L \right] Q^2 / 2 \tag{4b}$$

$$z_h \approx z_h^{hyd} = D_T Q^2 \tag{4c}$$

with c_s, D_T, and υ_L being, respectively, the adiabatic sound velocity, the thermal diffusivity, and the longitudinal kinematic viscosity.

One readily recognizes that Eq. (3) consists of these components (from left):

1. The so-called Rayleigh, or central, peak (term $\propto A_h$) which relates to entropy (heat) fluctuations diffusing at constant pressure (P).
2. The two Brillouin side peaks (term $\propto A_S$), connected to P-fluctuations propagating at constant entropy, and
3. An additional contribution (term $\propto A_S b$) asymmetric around the Brillouin peaks position having negative tails. This term distorts the Lorentzian terms (1) and (2) ultimately enabling the convergence of spectral moments $\int_{-\infty}^{+\infty} \omega^n S(Q, \omega) d\omega$ for $n \leq 2$. The latter imposes the following constraint: $b = [A_h z_h / (1 - A_h) + z_s] / \omega_s$.

The Rayleigh-Brillouin triplet in Eq. (3) is customarily quoted to as either generalized or simple hydrodynamic spectrum, respectively with or without the lowest order Q approximation in Eqs. (4a)–(4c).

It is worth stressing that the shape in Eqs. (3) and (4a)–(4c) provides an accurate description of the spectrum only when $D_T Q^2$, $\Gamma Q^2 << c_s Q$, or, equivalently, as long as the lifetime of hydrodynamic modes is much longer than the acoustic period. In this regime the spectrum is

dominated by three sharp peaks, forming the so-called Rayleigh-Brillouin triplet, typically measured in Brillouin light scattering (BLS) experiments.

Figure 2 displays the generic shape of the Rayleigh-Brillouin triplet from a liquid along with its three individual spectral components.

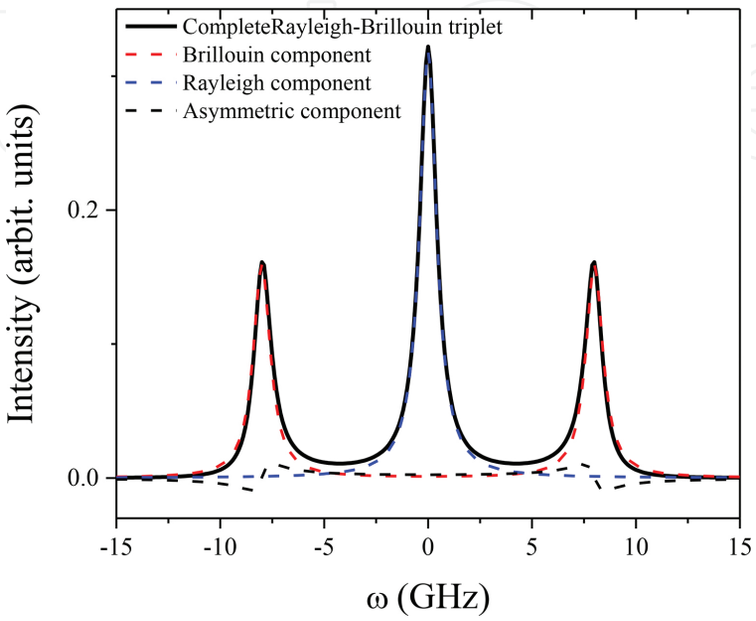

Figure 2. Typical shape of the Rayleigh-Brillouin triplet measured by Brillouin light scattering. The separate contributions to the total shape are represented by lines of different color, as indicated in the legend.

In general, the shape of the spectrum determined by a scattering experiment strongly depends on the probed space and time (or, equivalently, Q and ω) window, however the analytical form of such a dependence is generally unknown. Indeed, this is exactly known only at extreme Q and ω values: either extremely small (hydrodynamic limit-discussed above) or extremely large (single particle limit, to be discussed in Section 5).

At the crossover between these two limits, the shape of $S(Q,\omega)$ becomes highly sensitive complex dynamical processes involving inter and intramolecular degrees of freedoms. The coupling of density fluctuation with the mesoscopic dynamics of fluids makes the investigation of their spectrum of prominent interest.

3. The persistence of hydrodynamic modes beyond the continuous limit: first INS results

In principle, a "bare" extension of the hydrodynamic description of $S(Q,\omega)$ to the so-called mesoscopic regime would appear suspicious, since at those scales the matter can no longer be considered as continuous, or stationary. In fact, this regime corresponds to distances and times comparable with atomic separations and cage oscillations periods, respectively. Nonetheless,

sound arguments can still be used in support of a suitably generalized hydrodynamic description in this range. To understand this point, it is useful to recognize that for a dense liquid the mean free path can span the (10^{-1} nm) window, thus possibly becoming even smaller than interatomic separations. Under these conditions, the movements permitted to the atoms mainly resemble rapid, vibration-like, cage oscillations in the 0.1 ps window.

Consequently, even at mesoscopic (nm, ps) scales the response of the system is still "averaged" over a large number of elementary dynamic interactions, as required by a suitably generalized hydrodynamic description to hold validity. Based upon the above argument, possible reminiscences of Brillouin peaks in the THz spectrum of fluids appeared as an intriguing, yet somehow realistic, possibility since the early development of INS methods, which motivated several pioneering INS investigations in the mid-1960s.

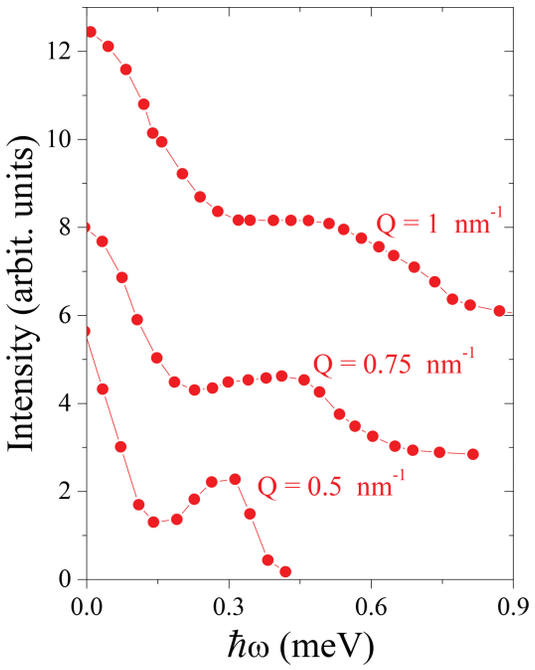

Figure 3. Few representative INS spectral line shapes of Ar measured by Bafile et al. [19] at low exchanged wave-vectors. Reported spectra have a mutual vertical offset for clarity.

Unfortunately, the first results reported in the literature were mutually inconsistent. In fact, the persistence in the spectrum of side shoulders reminiscent of hydrodynamic modes was suggested by Chen et al. [13] and successively confuted by Kroô et al. [14]. The former INS work focused on several samples having a strongly coherent neutron-scattering cross-section, as Ne, Ar, and D_2, and showed that, at low *Q*s, the frequency shift of side peaks approached from the above linear hydrodynamic law predicted by Eq. (4a) This pinpointed a link between these high frequency spectral features and the Brillouin peaks dominating the spectrum at much lower *Q*s. In a further INS work on Ar in both liquid (at $T = 94$ and 102 K) and solid (at $T = 68$ and 78 K) phases, Sköld et al. [15] found close resemblances between the phonon dispersion curves of a liquid and the one of a solid, thus suggesting that the local pseudo-periodicity of the liquid structure gives rise to quasiperiodic zones reminiscent of the Brillouin

http://dx.doi.org/10.5772/66126

zones of a crystal. A similar conclusion was previously reached by an INS investigation on liquid Pb [16], as well as a computer simulation on liquid Rb [17].

Coming back to noble gases, the first convincing evidence of well-defined inelastic peaks beyond the hydrodynamic regime is suggested by an INS measurement of Bell and collaborators on supercritical neon [18]. The low Q values explored in such a work ($0.6\ nm^{-1} \le Q \le 1.4\ nm^{-1}$) substantially reduced the dynamic gap between neutron and visible light Brillouin scattering techniques. The results demonstrated that the simple hydrodynamic theory consistently describes the spectral shapes well beyond the continuous limit and at least down to few nanometers distances. In particular, the inelastic shift of side peaks had, reportedly, a linear Q-dependence, whose slope is consistent with the adiabatic sound velocity.

Almost two decades after the measurement by Bell et al. on Ne, further low Q INS measurements were performed by Bafile et al. on supercritical Ar [19]. Again, the spectral line-shape measured in this work clearly confirmed the persistence of extended Brillouin peaks beyond the hydrodynamic limit (see **Figure 3**).

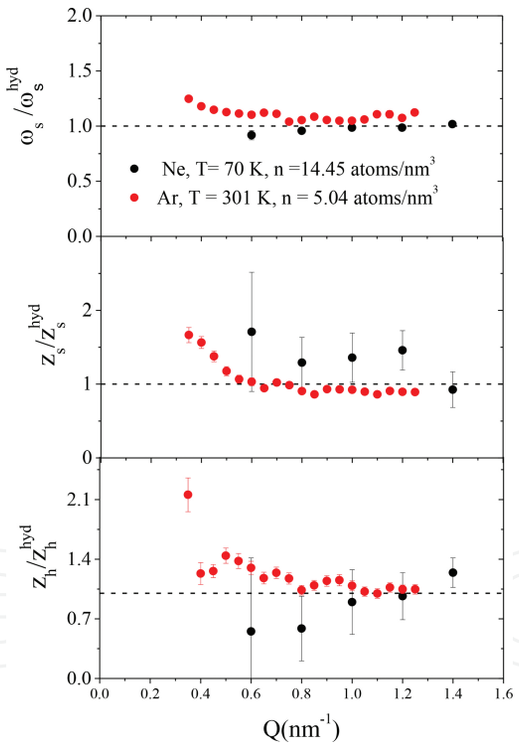

Figure 4. Shape parameters of the $S(Q,\omega)$ reported by Refs. [18, 19] for Ne and Ar, respectively, under the indicated thermodynamic conditions. Data are normalized to the corresponding hydrodynamic values as derived from Eqs. (4a)–(4c). Transport parameters in Eqs. (4a)–(4c) were extracted either from original works or from the database of the National Institute of Standards and Technology (NIST).

The extremely low Q range explored by this work ($0.35\ nm^{-1} \le Q \le 1.25\ nm^{-1}$) further reduced the gap separating standard INS measurements from light scattering ones. The INS investigation of Bafile and collaborators took full advantage of the improved statistical accuracy in

the beam counting and the unprecedented fine Q-grid. Both these assets enabled a very precise determination of the Q-dependence of line-shape parameters in Eq. (3).

Best-fit values of such parameters derived from [19] are reported in **Figure 4** after normalizations to the respective simple hydrodynamic predictions, expressed by Eqs. (4)–(4). The corresponding quantities derived by Bell and collaborators for neon [18] are also reported for comparison.

Data reported in **Figure 4** demonstrate that the simple hydrodynamic laws in Eqs. (4a)–(4c) derived for continuous media hold validity up to the ≈ 1 nm^{-1} mesoscopic Q-range. This result is certainly surprising since at these Q's the spectral peaks gradually transform into broad features (see, e.g., **Figure 3**) for which the simple hydrodynamic approximation ($D_T Q^2$, $\Gamma Q^2 << c_s Q$) becomes clearly inaccurate. In Ref. [19] these high frequency inelastic features are quoted to as "extended hydrodynamic modes," which emphasizes their hydrodynamic-like behavior persistent well beyond the continuous limit.

4. The advent of inelastic X-ray scattering

The only *THz* spectroscopic technique available until the mid-1990s, INS, is intrinsically hampered by kinematic limitations (see, e.g., [5] pp. 63–101). These shrink the accessible portion of dynamic plane (Q,ω) especially at low Qs, where the collective modes dominate. This problem was successfully addressed by the development of IXS, a technique virtually free from kinematic limitations [2, 3], apart from, of course, those arising from finite energy resolution width. Toward the end of past millennium, the availability of this new spectroscopic tool revitalized the interest toward experimental studies of the transition from the continuous to the mesoscopic regime. It is important to stress that noble gases present undoubted advantages in this kind of studies. In fact, at variance of molecular fluids, their microscopic components lack internal degrees of freedom and contrary to, e.g., metallic liquids, microscopic interactions are simpler and shorter-ranged. These, for instance, are key assets to reliably approximate the interatomic potential when performing molecular dynamics (*MD*) simulation studies [20]. Another advantage of gaseous systems in general is the large compressibility, which permits substantial variations of density, that is the strength of atomic interactions, even with moderate thermodynamic changes.

The first IXS measurement on a dense noble gas was performed on deeply supercritical neon (T = 295 K, n = 29.1 atoms/nm^3) in 1998. Experimental results were discussed in combination with the outcome of a parallel *MD* simulation on a Lennard-Jones model representative of the same sample [21]. In **Figure 5**, some of the IXS spectra discussed in this work (and, successively in Ref. [22]) are compared with the best-fitting line-shape obtaining using Eq. (3) as a model, without any constraint on the Q dependence of shape parameters. In this case the persistence of a triple peak structure at mesoscopic scale can be inferred at least up to Q = 6 nm^{-1}, while at Q = 10 nm^{-1} or higher the two shoulder can be no longer easily discerned in the IXS spectral shape.

http://dx.doi.org/10.5772/66126

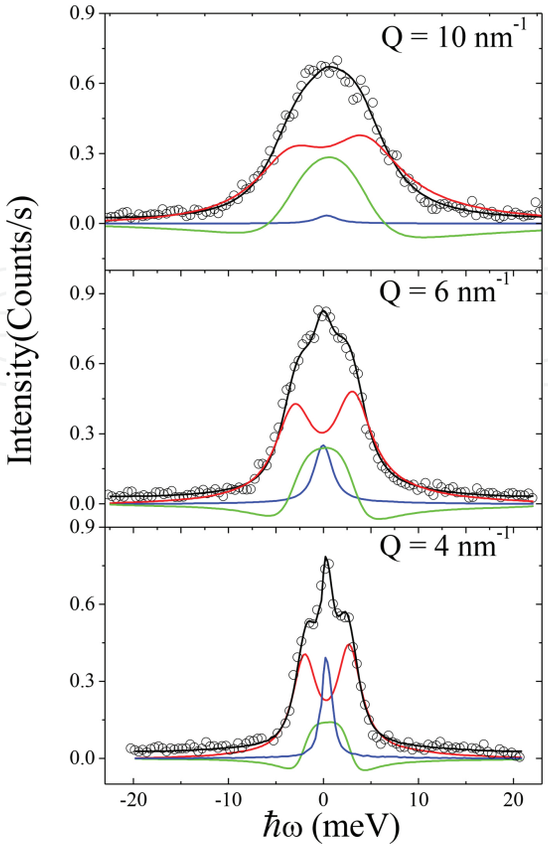

Figure 5. Some representative spectral shapes (circles) of deeply supercritical neon at P = 3 kbar and ambient temperature reported in [22] are compared with corresponding best-fitting line shapes (black lines) and their quasi-elastic (blue), inelastic (red) and "negative tails" (green line) components. These are obtained using Eq. (3) as a model for the spectral shape.

4.1. The Q-dependence of the spectral shape parameters

At this stage a question may arise on the Q dependence of inelastic peaks beyond the extremely low Q (<1nm^{-1}) extended hydrodynamic regime probed by Brillouin neutron scattering. A meaningful answer to this question is provided by the IXS results displayed in **Figure 6**, which illustrates the results reported in [21] and also discussed in [22]. These data refer to deeply supercritical neon at room temperature and 3 Kbar pressure. Plotted data appear paradigmatic of an IXS measurement on a simple, hard sphere-like, system of a supercritical dense gas. The curves are compared with the trends expected in the simple hydrodynamic limit, as obtained by inserting in Eqs. (4a)–(4c) the transport parameters derived from the National Institute of Standards and Technology (NIST). It can be readily noticed that the Q-dependence of ω_s is linear within a Q range extending up to $Q \approx 10$ nm^{-1}, the slope being consistent with the adiabatic sound velocity of the sample (1050 m/s). The Q-interval spanned by this linear trend corresponds to distances larger than about .6 nm, a value higher, yet comparable, with first neighboring atoms separations. This indicates that an extended hydrodynamic behavior can be still observed at Q higher by a decade than those previously investigated by Bell et al. [18] and Bafile et al. [19].

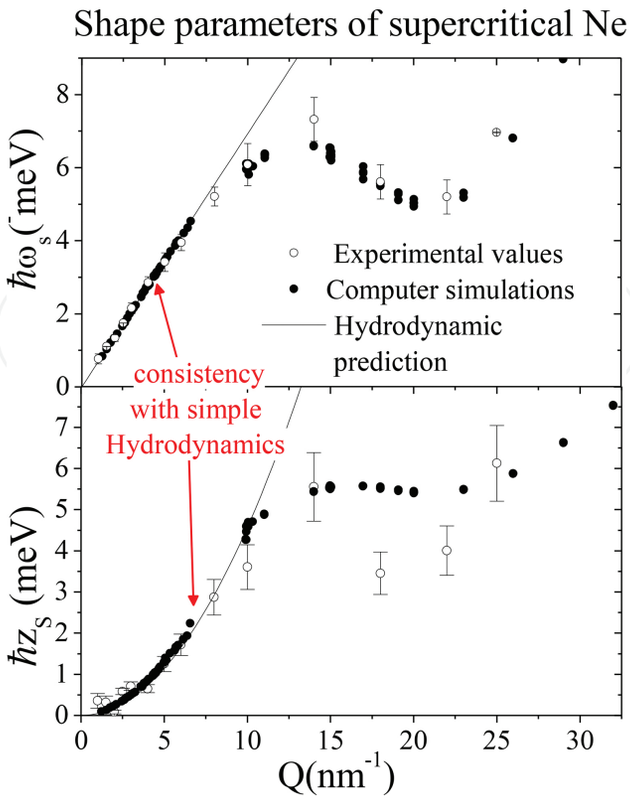

Figure 6. Shape parameters of the inelastic modes of *S(Q,ω)*, as derived for supercritical Ne by IXS (circles [22]) and MD simulations (dots [21]). The solid lines represent the hydrodynamic predictions derived from Eqs. (4a) and (4b), while inserting in them thermodynamic and transport parameters from [28] and from [29], respectively.

4.1.1. The role of the static structure factor

From **Figure 6** one readily notices that beyond $Q = 10$ nm^{-1} the extended acoustic frequency ω_s bends down to a minimum at about 22.5 nm^{-1}. This turns out to be the same Q value where the structure factor *S(Q)* (not reported in the plot) reaches its first maximum. We recall here that the static structure factor is related to the *S(Q,ω)* by the simple relation:

$$S(Q) = \int_{-\infty}^{\infty} S(Q,\omega)\, d\omega \tag{5}$$

Upon inserting Equation (1) i the formula above, it readily appears that the ω-integration of *S(Q,ω)* introduces a term $\propto \delta(t) = 1/2\pi \int_{-\infty}^{\infty} \exp[i\omega t]dt$, which, as well known, is nonvanishing only for $t = 0$. It follows that *S(Q)* essentially measures the "static" ($t = 0$) value of density correlations, rather than the dynamic one probed by *S(Q,ω)*. Therefore, *S(Q)* carries direct insight into time-independent or structural properties of the fluid, which justify the name "static structure factor," customarily used for this variable. Alternatively, *S(Q)* is often referred to as diffraction

profile as directly determined by diffraction measurements. These are frequency integrated measurements of the scattering and, as such, not directly sensitive to the dynamic (*t*-dependent) properties of the sample.

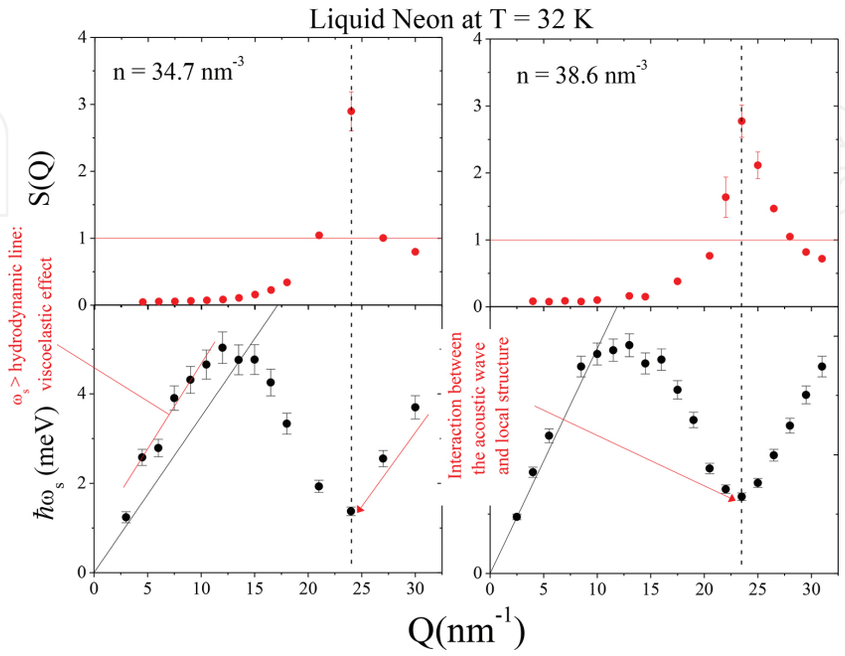

Figure 7. The dispersion liquid neon (bottom panels) are compared with the diffraction profiles *S(Q)* (upper panels), both being derived from IXS measurements discussed in Ref. [24] The vertical dashed lines indicates the essentially coincident *Q*-position of minima and maxima of ω_s and *S(Q)*, respectively. Horizontal lines in the upper plots indicate the asymptotic large *Q* unit value. The dispersive effects discussed in the text are labeled and indicated by arrows.

Typical *S(Q)* profiles of a liquid are reported in **Figures 7** and **9**. In all reported curve one readily notices the presence of a sharp maximum at some exchanged wavevector, $Q = Q_m$ for which $Q_m = 2\pi/a$, with a being the average distance between first neighboring atoms. Furthermore, it clearly appears from **Figure 9** that beyond the first diffraction peak the *S(Q)* displays oscillations from the unit limiting value, which is reached at extremely high *Q*'s. As discussed in Section 5 in further detail, these oscillations are induced by coherent or "pair" interactions. In crystalline solid pair, interactions are much stronger and this is reflected by the circumstance that the diffraction profile, rather than highly damped oscillations, displays narrow and exceptionally intense spots (Bragg peaks) [23].

4.2. The physical meaning of the dispersion minimum

The coincidence between the positions of the first *S(Q)* maximum and the ω_s minimum is an ubiquitous feature of liquids, clearly exemplified in **Figure 7**. There, the dispersion curve and corresponding static structure factor are compared as derived from the modeling of IXS spectra of liquid Ne [24]. The vertical dashed line shows unambiguously the coincidence between the *S(Q)* maximum and ω_s minimum. Indeed, both effects appear as a manifestation of the interference between the density fluctuations and the pseudo-periodicity of the local structure.

Specifically, a maximum in *S(Q)* is observed when the probed distance, Q^{-1}, roughly matches the first neighboring atoms' separation. Under this condition, the presence of an "interference node" (the first neighboring atom) causes a sharp minimum in the density wave dispersion.

This minimum arises from the coexistence of an acoustic wave "transmitted" through the node — for which $\partial\omega_s/\partial Q > 0$ (positive group velocity)—and one reflected by it— for which $\partial\omega_s/\partial Q < 0$ (negative group velocity). It is commonly observed that the sharpness of this minimum deeply enhances upon approaching the solid phase. This suggests that, at mesoscopic scales, dispersion of a dense liquid resembles the one of its crystalline counterpart.

4.3. The slowing down of the dynamics

Figure 6 clearly shows that beside the extended sound frequency ω_s, also the half-width of the sound mode, $z_{s,}$ reaches a local minimum at Q_m and, although non reported in the figure, a similar behavior is observed for the quasielastic half-width z_h [25]. The occurrence of a minimum in z_h was predicted by De Gennes [26], the effect having been named after him the "De Gennes narrowing." More in general, a large body of IXS results on liquids demonstrates that all relevant timescales defining the dynamics of density fluctuations undergo a clear enhancement at Q_m. This global slowing down of the dynamics stems from the higher correlation between the movements of the atoms and those of the respective first neighbor cages for $Q = Q_m$. As noticed by Sköld [27] *S(Q)* yields a measure of the effective number of atoms contributing to the scattered intensity at a given exchanged wave vector Q. It seems thus natural to ascribe the slowing down at Q_m to the higher inertia of the target system due to the larger number of atoms participating to the collective response of the target system. In particular, first neighbor movements become more correlated when Q matches the inverse of first neighbor's separations and *S(Q)* approaches its first maximum. One can thus identify the quantity $Q^* = Q/\sqrt{S(Q)}$ as the momentum "effectively" transferred, where the factor $\sqrt{S(Q)}$ embodies the inertia of the target system [27]. For a perfect crystal, owing to the global periodicity of first neighbors' arrangement, such a factor diverges when Bragg conditions are met. Here the whole target system coherently participates to density fluctuations and, correspondingly, an infinitely narrow intrinsic spectral linewidth is to be expected. Furthermore, the effective inelastic shift, proportional to Q^*, tends to vanish as $1/\sqrt{S(Q)}$.

4.4. The onset of viscoelastic effects

A noticeable feature displayed by the left bottom plot of **Figure 7** is the clear inconsistency between the low-intermediate Q region of the dispersion curve and the corresponding linear hydrodynamic prediction.

Although a detailed description of this effect goes beyond the scope of this chapter, it is useful to recall here that this is a manifestation of the viscoelastic response induced by the coupling with a relaxation process.

To better illustrate this point, it is useful to recall that scattering-excited density fluctuation causes a time-dependent perturbation of the local equilibrium of the target sample. As a

http://dx.doi.org/10.5772/66126

response, decay channels redistribute the energy from the density fluctuation toward some internal degrees of freedom, thus ultimately driving the sample to relax into a new local equilibrium within a timescale τ.

Two limiting scenarios can thus occur:

1. the time-dependent acoustic perturbation has a timescale much longer than any internal degrees of freedom of the system. Under these conditions, the latter relaxes to equilibrium "instantaneously" and the density fluctuation propagates or diffuses over successive equilibrium states (**viscous**, or liquid-like, limit);
2. If the density fluctuation is instead extremely rapid, it "perceives" internal rearrangements as frozen-like and does not couple with them thus virtually evolving with no energy losses (**elastic** or solid-like limit).

If such considered perturbation has the form of an acoustic wave, its transition from the viscous to the elastic limit is accompanied by a decrease of dissipation and a consequent increase in the propagation speed. Therefore a **viscoelastic** transition manifests itself through a systematic increase of sound velocity with Q. While the hydrodynamic theory correctly predicts (through Eq. (4a)) the Q-dependence of ω_s in the viscous limit, it fails to predict its elastic value at intermediate Qs. This explains the discrepancy between the hydrodynamic straight line and the actual value of the inelastic shift in the 5 $nm^{-1} < Q < 14$ nm^{-1} range, as evidenced in the bottom left plot of **Figure 7**.

5. Moving toward the single particle limit

Upon reaching extremely high Q values, the probed dynamic event gradually reduces to the free recoil of the single particle after the collision with the probe particle and before any successive interactions with the first neighbors' cage.

Within these short times, the struck atom can be assumed to freely stream without interacting with the neighboring cage, its equation of motion being thus expressed as $\vec{R}_j(t)=\vec{v}_j t$.

This merely "ballistic" behavior can be easily understood for a system of hard spheres, in which microscopic interactions essentially consists of atomic collisions, i.e., interactions instantaneous and localized in space. For a more realistic system, atomic interactions can no longer be considered as "close contact", rather spanning finite distance and time lapses. However, if the energy transferred in the scattering event is much larger than any local interaction, the struck particle can still be "perceived" as freely recoiling from the collision with the probe. In this so-called impulse approximation (IA) regime it can be safely assumed that no sizable external force acts on the isolated system formed by the incident photon and the struck atom.

Within the unrealistic hypothesis that the target atom is exactly at rest, its response function would reduce to a delta function centered at the recoil energy. More realistically, one can assume that the initial state of the system is characterized by a distribution of initial momenta, and the spectrum scattered by this moving source therefore becomes "Doppler broadened."

Each possible initial momentum provides a contribution to the scattering intensity and the shape of the spectrum is directly connected to the momentum distribution of the struck particle.

For a classical particle this can be assumed to have the form of a Maxwell-Boltzmann distribution $\propto \exp\left(-Mv^2/2k_BT\right)$, where M is the atomic mass. Disregarding the analytical details of the derivation (thoroughly discussed, for instance, in Ref. [5]), it is here important to mention that the use of the Boltzmann distribution ultimately yields the following Gaussian shape for the dynamic structure factor:

$$S_{IA}(Q,\omega) = \left(\frac{M}{2\pi k_B T Q^2}\right)^{1/2} \exp\left[\frac{M\hbar}{2\pi k_B T Q^2}(\omega-\omega_r)^2\right] \tag{6}$$

where the suffix "IA" labels the impulse approximation value of $S(Q,\omega)$. One readily recognizes that profile in Eq. (8) is a Gaussian centered at $\omega=0$ and its variance, k_BTQ^2/M, can be simply related to the mean kinetic energy of the struck particle ($\langle K.E.\rangle = 3/2k_BT$ for a monatomic system). It can be shown that for a quantum system, the *IA* spectrum preserves the Gaussian shape; however, its variance deviates from the classically expected values being instead simply determined by the quantum value of $\langle K.E.\rangle$. Since the latter is in general unknown, a useful application of extremely high Q measurements is to achieve a direct determination of its value (see, e.g., Ref. [30]). Another interesting application is the determination of actual shape of the momentum distribution, e.g., in intriguing quantum system as Bose condensates [31].

The study of the spectrum of simple fluids in the IA regime [32] has been for decades an essentially exclusive domain of deep inelastic neutron scattering (DINS). The first deep inelastic X-ray scattering (DIXS) investigations of the IA spectrum of liquids were pioneered by a work on liquid neon at the onset of the new millennium [33].

In this work, it was found that the single particle kinetic energy extracted from the spectral shape provided clear evidence for quantum deviations.

An example of the gradual evolution of the IXS spectrum toward the single particle Gaussian shape predicted by Eq. (6) is illustrated in **Figure 8**.

DIXS experiments are not common in the literature since this technique suffers from major intensity penalties due to the high Q decay of the form factor. Furthermore, these studies often deal with samples having a light atomic mass (as He, D_2 and H_2, and Ne), as better suited to observe quantum effects. Unfortunately, these systems have also a small atomic number which makes their IXS cross-section rather weak. Finally, the highest Q's reachable by DIXS are still below typical values covered by DINS measurements by more than an order of magnitude. These intrinsic and practical difficulties explain why DIXS experiments are still sporadic and this technique is still in its "infancy."

http://dx.doi.org/10.5772/66126

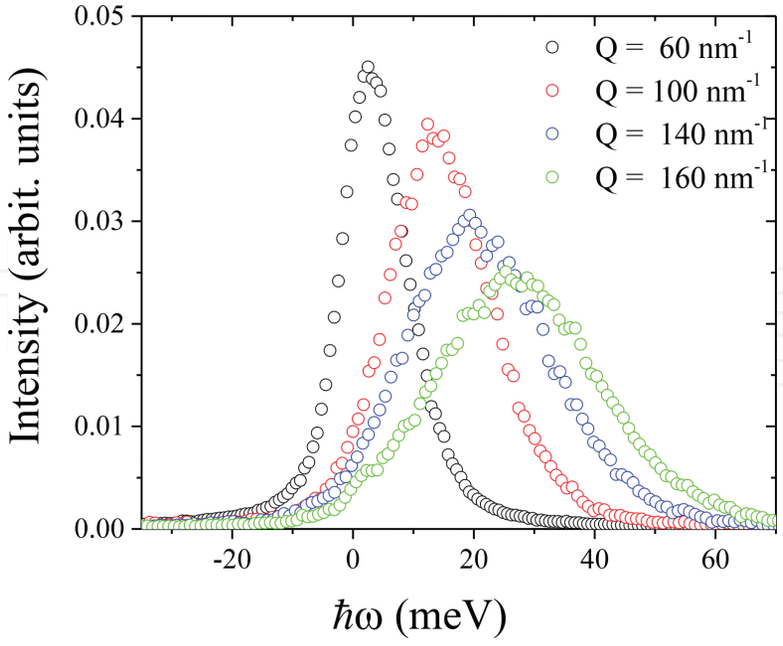

Figure 8. The gradual *Q*-evolution of the IXS spectrum of Ne [33] toward the Gaussian shape characteristic of the single particle regime.

It is important to stress that the IA regime is only joined asymptotically at extremely high *Q*s. Before this limit is fully reached, the struck atom cannot be considered as a freely recoiling object and first neighbor interactions need to be taken into account explicitly. It is usually assumed that the latter influence only the final (after scattering) state of the struck particle, while its initial state being still essentially "free." Among various recipes to handle theoretically these "final state effects," the so-called additive approach [34], is the one used in the very few extremely high *Q* IXS measurements available [33, 35, 36]. This approach stems from an expansion of the intermediate scattering function in time cumulants, in which only the first few lower order term are retained. As a results of this perturbative treatment, deviations from a perfect Gaussian shape can be easily linked to the lowest order (n) spectral moments and contain valuable information on meaningful physical parameters as, e.g., the mean force acting on the atom and the mean square Laplacian, both providing a meaningful and unique characterization of quantum effects (see, e.g., [33]).

5.1. The case of molecular systems

After the work of Monaco et al. on a monoatomic fluid [33], a successive *D*IXS work [35] aimed at investigating the next simplest case of a diatomic homonuclear system as liquid iodine. In this work, no signature of quantum effects was reported due to both the larger molecular mass and the higher temperature of the sample.

Even in the absence of quantum deviations, the interpretation of the IXS spectrum of a molecular fluid is overly complex, owing to the coupling of the spectroscopic probe with all molecular degrees of freedom [37] as well as their mutual entanglement. In the simplest assumption that all degrees of freedom are decoupled and belong to very disparate energy

windows, the observed response strongly depends on how the exchanged energy, E compares not only with centers of mass translational energies, E_t, but also with intramolecular rotational and vibrational quanta, $\hbar\omega_r$ and $\hbar\omega_v$, respectively.

Specifically, three complementary *IA* regimes can be identified:

- When $E_t << E << \hbar\omega_r, \hbar\omega_v$ the struck molecule is "seen" by the probe as an object with spherical symmetry experiencing a merely translational recoil induced by the collision with the probe. The energy of such a recoil energy is $\hbar^2 Q^2 / 2M$, with M being the molecular mass. Here the scattered intensity carries direct insight into the merely translational momentum distribution of the molecular centers of mass.

  In an intermediate window ($E_t, \hbar\omega_r << E << \hbar\omega_v$), usually referred to as the $Sachs-Teller\,(ST)$ regime [38], the molecule behaves as a freely recoiling rigid roto-translator. In this Sachs-Teller regime, the rotational component of the recoil can be written as $\hbar^2 Q^2 / 2M_{ST}$, in which the effective, or Sachs-Teller mass, M_{ST}, is determined by the eigenvalues of the molecular tensors of inertia. In this regime, the spectral density becomes proportional to the distribution of roto-translational momenta of the molecules. The DIXS work in Ref. [35] demonstrated that the Sachs-Teller theory provides a consistent interpretation of the spectral shape of iodine at the largest Q values covered by state-of-art IXS spectrometers.

- Eventually, when the $E >> \hbar\omega_{r,v}$ condition is matched, the exchanged energy becomes overwhelmingly stronger than any intramolecular and intermolecular interaction, therefore, the nucleus inside the molecule is for short-time freed from its bound state experiencing a recoil as a free particle. Under these conditions, the scattering intensity becomes proportional to the single proton initial momentum distribution.

  In principle, at higher exchanged energies and momenta higher-level IA regimes can be probed. This happens when energies transferred in the scattering event are much larger than intranuclear interaction and, correspondingly, subnuclear particle start experiencing free particle recoils. These phenomena belong to a domain of physics complementary to condensed matter Physics and rather fitting in the fields of high energy and particle physics.

6. Summarizing the state of the art of IXS technique

In conclusion, the relevant phenomenology of the spectral evolution from the hydrodynamic to the single particle regime discussed in this chapter is summarized in **Figure 9**. There, the whole crossover of the spectral shape from the hydrodynamic Brillouin triplet to the single particle Gaussian is reported as determined in separate inelastic measurements. The corresponding Q window are indicated in reference to the various regions of the diffraction profile *S(Q)*, reported in the center of the figure. It can be readily noticed that, while "climbing" the wings of the first diffraction peak, the sharp Brillouin triplet (Panel A) gradually transforms into a more complex shape in which the side peaks appear as broad features (Panels B). When Q values become comparable or higher than the position of the dominant S(Q) peak (Panel C),

http://dx.doi.org/10.5772/66126

these shoulder can no longer be resolved due to their intrinsic overdamping. The best-fit components of the spectrum, also reported for the spectra in Panel C, can help to better identify the presence of these "generalized hydrodynamic" modes. Upon further increasing *Q*, "coherent" oscillations of *S(Q)* gradually damp out and correspondingly the shape of the spectrum transforms into a Gaussian centered at the recoil energy (Panel D). This gradual evolution can be readily captured by comparing the measured shape with the Gaussian profile in Eq. (6).

Great expectations are raised by the advent of new generation IXS spectrometers further reducing the dynamic gap separating IXS from Brillouin light scattering [39]. This will possibly revitalize the dream of entire generations of condensed matter physicists: a single inelastic spectrometer covering the relevant portion of the crossover from the hydrodynamic to the single particle regimes. Parallel advances in the theory of the spectrum of fluids and the empowering of simulation methods are deemed to improve our understanding of this crossover and all dynamical phenomena happening in a fluid from macroscopic to microscopic scales.

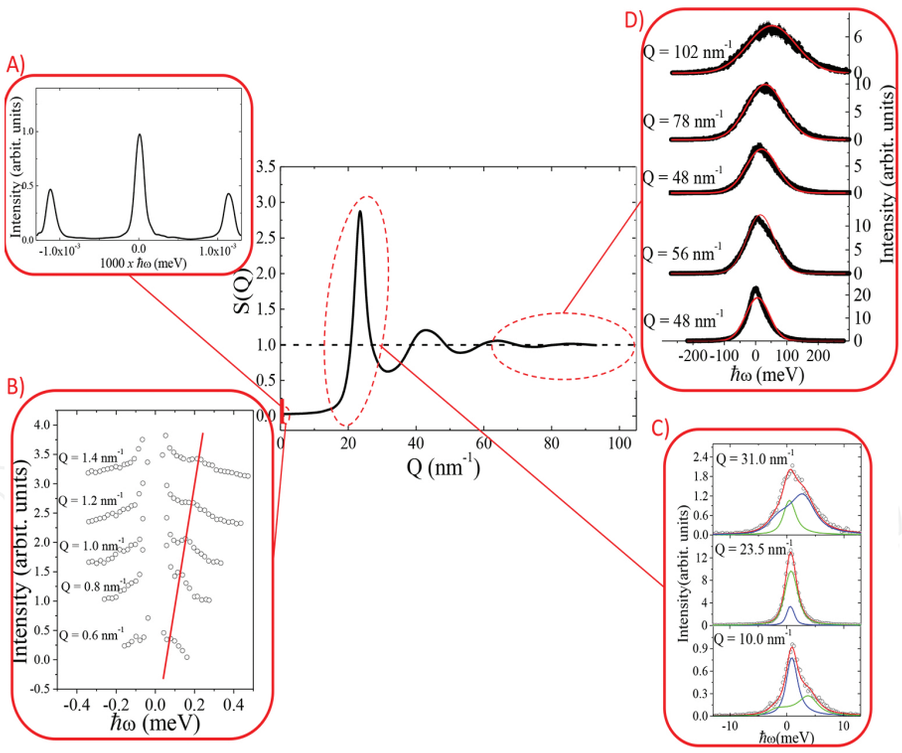

Figure 9. Overview of experimental spectra measured in several *Q* windows across the transition from the hydrodynamic to the single particle regime in monatomic fluids. Panel A reports Brillouin light scattering spectra of liquid Ar [40]. Panel B displays INS measurements on supercritical Ne [18] with the red line roughly indicating the linear dispersion of side peaks. Panel C shows IXS spectra on liquid Ne [24]) with corresponding best-fitting line shapes and individual spectral components. Finally, Panel D displays IXS spectra of liquid Li from [41] along with the single particle Gaussian shape (red line) predicted by Eq. (9).

Acknowledgements

This work used resources of the National Synchrotron Light Source II, a U.S. Department of Energy (DOE) Office of Science User Facility operated for the DOE Office of Science by Brookhaven National Laboratory under contract no. DE-SC0012704.

Author details

Alessandro Cunsolo

Address all correspondence to: acunsolo@bnl.gov

National Synchrotron Light Source II, Brookhaven National Laboratory, Upton, NY, USA

References

[1] Brockhouse BN, Stewart AT. Scattering of neutrons by phonons in an aluminum single crystal. Physical Review. 1955; 100: 756–757. DOI: http://dx.doi.org/10.1103/PhysRev.100.756

[2] Burkel E. Phonon spectroscopy by inelastic X-ray scattering. Reports on Progress in Physics, 2000; 63: 171–232. DOI: http://dx.doi.org/10.1088/0034-4885/63/2/203

[3] Krisch M, Sette F. in Neutron and X-Ray Spectroscopy. Berlin: Springer-Verlag; 2007. pp. 317–370.

[4] Berne BJ, Pecora R. Dynamic Light Scattering. Mineola: Dover; 1976. 384 p.

[5] Lovesey SW. Theory of Neutron Scattering from Condensed Matter. Vol. 1. Oxford: Clarendon Press; 1984. 329 p.

[6] Sinha SK. Theory of inelastic X-ray scattering from condensed matter. Journal of Physics-Condensed Matter, 2001; 13: 7511–7523.

[7] Cunsolo A. Using X-ray as a probe of the terahertz dynamics of disordered systems —complementarity with inelastic neutron scattering and future perspectives. in Neutron Scattering, WA Monteiro, Editors. Rjeka: InTech; 2016.

[8] Jackson JD. Classical Electrodynamics. Vol. 3. New York: Wiley; 1962.

[9] Brillouin L. Diffusion of light and X-rays by a transparent homogeneous body. Annales de Physyque (Paris), 1922; 17: 88.

[10] Mason EA, Marrero TR. The diffusion of atoms and molecules, in Advances in Atomic and Molecular Physics, Bates DR, Immanuel E, Editors. Orlando: Academic Press; 1970. pp. 155–232.

[11] Hansen, JP, IMcDonald IR. Hydrodynamics and transport coefficients, in Theory of Simple Liquids (Third edition), Chapter 8. Burlington: Academic Press; 2006. pp. 219–254.

[12] Bafile U, Guarini E, Barocchi F. Collective acoustic modes as renormalized damped oscillators: unified description of neutron and X-ray scattering data from classical fluids. Physical Review E. 2006; 73: 061203 DOI: http://dx.doi.org/10.1103/PhysRevE.73.061203.

[13] Chen SH, et al. Co-operative modes of motion in simple liquids. Physics Letters. 1965; 19: 269–271. DOI: 10.1016/0031-9163(65)90980-7

[14] Kroô N, et al. International Atomic Energy Agency. Inelastic scattering of cold neutrons by condensed argon. in Symposium on Inelastic Scattering of Neutrons. Bombay: IAEA; 1964.

[15] Skold K, Larsson KE. Atomic motion in liquid argon. Physical Review. 1967; 161: 102–116.

[16] Randolph PD, Singwi KS. Slow-neutron scattering and collective motions in liquid lead. Physical Review. 1966; 152: 99–112.

[17] Rahman A. Propagation of density fluctuations in liquid rubidium: a molecular-dynamics study. Physical Review Letters. 1974; 32: 52–54.

[18] Bell HG, Kollmar A, Alefeld B, Springer T. Investigation of collective excitations in liquid neon by means of neutron-scattering at small scattering vectors. Physics Letters A. 1973; 45: 479–480. DOI: 10.1016/0375-9601(73)90717-2

[19] Bafile U, Verkerk P, Barocchi F, de Graaf LA, Suck JB, Mutka H. Onset of departure from linearized hydrodynamic behavior in argon gas studied with neutron Brillouin scattering. Physical Review Letters. 1990; 65: 2394–2397. DOI: http://dx.doi.org/10.1103/PhysRevLett.65.2394

[20] Allen MP, Tildesley DJ. Computer Simulation of Liquids. Oxford: Oxford University Press; 1989.

[21] Cunsolo A, Pratesi G, Ruocco G, Sampoli M, Sette F, Verbeni R, Barocchi F, Krisch M, Masciovecchio C, Nardone M. Dynamics of dense supercritical neon at the transition from hydrodynamical to single-particle regimes. Physical Review Letters. 1998; 80: 3515–3518. DOI: http://dx.doi.org/10.1103/PhysRevLett.80.3515

[22] Cunsolo A. Relaxation Phenomena in the THZ Dynamics of Simple Fluids Probed by Inelastic X Ray Scattering. Grenoble: Universite' J. Fourier; 1999.

[23] Egami T, Billinge SJ. Underneath the Bragg Peaks: Structural Analysis of Complex Materials. Vol. 16. Oxford: Elsevier; 2003.

[24] Cunsolo A, Pratesi G, Verbeni R, Colognesi D, Masciovecchio C, Monaco G, Ruocco G, Sette F. Microscopic relaxation in supercritical and liquid neon. Journal of Chemical Physics, 2001; 114: 2259–2267. DOI: http://dx.doi.org/10.1063/1.1334613

[25] Cunsolo A, Pratesi G, Rosica F, Ruocco G, Sampoli M, Sette F, Verbeni R, Barocchi F, Krisch M, Masciovecchio C, Nardone M. Is there any evidence of a positive sound dispersion in the high frequency dynamics of noble gases? Journal of Physics and Chemistry of Solids. 2000; 61: 477–483. DOI: http://dx.doi.org/10.1016/S0022-3697(99)00340-6

[26] De Gennes PG. Liquid dynamics and inelastic scattering of neutrons. Physica. 1959; 25: 825–839. DOI: 10.1016/0031-8914(59)90006-0

[27] Skold K. Small energy transfer scattering of cold neutrons from liquid argon. Physical Review Letters. 1967; 19: 1023–1025. DOI: http://dx.doi.org/10.1103/PhysRevLett.19.1023

[28] NIST. Thermodynamic data are from the database *http://webbook.nist.gov/chemistry/form-ser.html*.

[29] Castillo R, Castaneda S. The bulk viscosity in dense fluids. International Journal of Thermophysics. 1988; 9: 383–390. DOI: 10.1007/BF00513078

[30] Senesi R, Andreani C, Colognesi D, Cunsolo A, Nardone M. Deep-inelastic neutron scattering determination of the single-particle kinetic energy in solid and liquid 3He. Physical Review Letters. 2001; 86: 4584–4587. DOI: http://dx.doi.org/10.1103/PhysRevLett.86.4584

[31] Stringari, S, Pitaevskii L, Stamper-Kurn DM, Zambelli F. Momentum distribution of a bose condensed trapped gas, in Bose-Einstein Condensates and Atom Lasers, S Martellucci, et al., Editors. Boston: Springer; 2002. pp. 77–95.

[32] Silver RN, Sokol PE, Editors. Momentum Distributions. New York: Springer; 2013.

[33] Monaco G, et al. Deep inelastic atomic scattering of X rays in liquid neon. Physical Review Letters. 2002; 88: 227401. DOI: http://dx.doi.org/10.1103/PhysRevLett.88.227401

[34] Glyde HR. Momentum distributions and final-state effects in neutron scattering. Physical Review B. 1994; 50: 6726–6742. DOI: http://dx.doi.org/10.1103/PhysRevB.50.6726

[35] Izzo, MG, Bencivenga F, Cunsolo A, Di Fonzo S, Verbeni R, Gimenez De Lorenzo R. The single particle dynamics of iodine in the Sachs-Teller regime: an inelastic X ray scattering study. Journal of Chemical Physics. 2010; 133: 124514. DOI: 10.1063/1.3483689

[36] Cunsolo A, Monaco G, Nardone M, Pratesi G, Verbeni R. Transition from the collective to the single-particle regimes in a quantum fluid. Physical Review B. 2003; 67: 024507. DOI: http://dx.doi.org/10.1103/PhysRevB.67.024507 38

[37] Krieger TJ, Nelkin MS. Slow neutron scattering by molecules. Physical Review. 1957; 106: 290–295. DOI: http://dx.doi.org/10.1103/PhysRev.106.290

[38] Sachs RG, Teller E. The scattering of slow neutrons by molecular gases. Physical Review. 1941; 60: 18–27. DOI: http://dx.doi.org/10.1103/PhysRev.60.18

[39] Cai YQ, Coburn1 DS, Cunsolo A, Keister JW, Honnicke MG, Huang XR, Kodituwakku CN, Y Stetsko1, Suvorov A, Hiraoka N. The ultrahigh resolution IXS beamline of nsls-ii: recent advances and scientific opportunities. 11th International Conference on Synchrotron Radiation Instrumentation (Sri 2012), 2013; 425: 202001. DOI: http://dx.doi.org/10.1088/1742-6596/425/20/202001

[40] Fleury PA, Boon JP. Brillouin Scattering in Simple Liquids – Argon and Neon. Physical Review. 1969; 186:244–254. DOI: https://doi.org/10.1103/PhysRev.186.244

[41] Scopigno T, Balucani U, Cunsolo A, Masciovecchio C, Ruocco G, Sette F, Verbeni R. Phonon-like and single-particle dynamics in liquid lithium. Europhysics Letters. 2000; 50:189–195. DOI: 10.1209/epl/i2000-00253-5

IntechOpen